Structure, Vol. 10, 1261–1272, September, 2002, ©2002 Elsevier Science Ltd. All rights reserved. PII S0969-2126(02)00826-2

Gene Sequence and the 1.8 Å Crystal Structure of the Tungsten-Containing Formate Dehydrogenase from *Desulfovibrio gigas*

Hans Raaijmakers,[1,4,5] Sofia Macieira,[1,2,4] João M. Dias,[1] Susana Teixeira,[1] Sergey Bursakov,[1] Robert Huber,[2] José J.G. Moura,[1] Isabel Moura,[1] and Maria J. Romão[1,3]

[1]REQUIMTE/CQFB
Departamento de Química
FCT
Universidade Nova de Lisboa
2829-516 Caparica
Portugal

[2]Max-Planck-Institut für Biochemie
Am Klopferspitz 18a
D-82152 Martinsried
Germany

Summary

***Desulfovibrio gigas* formate dehydrogenase is the first representative of a tungsten-containing enzyme from a mesophile that has been structurally characterized. It is a heterodimer of 110 and 24 kDa subunits. The large subunit, homologous to *E. coli* FDH-H and to *D. desulfuricans* nitrate reductase, harbors the W site and one [4Fe-4S] center. No small subunit ortholog containing three [4Fe-4S] clusters has been reported. The structural homology with *E. coli* FDH-H shows that the essential residues (SeCys158, His159, and Arg407) at the active site are conserved. The active site is accessible via a positively charged tunnel, while product release may be facilitated, for H^+ by buried waters and protonable amino acids and for CO_2 through a hydrophobic channel.**

Introduction

Formate dehydrogenases (FDHs) are a heterogeneous group of enzymes found in prokaryotes and eukaryotes. They catalyze the reversible two-electron oxidation of formate to carbon dioxide. In aerobic organisms FDHs are mainly NAD^+-dependent enzymes, while, in anaerobic bacteria, they comprise a variety of proteins that contain a complex inventory of redox centers and are very sensitive to oxygen. This is not the case for *Desulfovibrio gigas* formate dehydrogenase (*Dg*W-FDH), which, unlike other FDHs, loses activity in the presence of air, but this activity can be restored [1, 2]. Formate dehydrogenases have been isolated from other sulfate reducers, such as *Desulfovibrio vulgaris* Hildenborough (*Dv*FDH), which contains three subunits (α, β, and γ). Subunits α and β are similar to those from *Dg*W-FDH, but, instead of W, the enzyme contains Mo [3]. The γ subunit is a multiheme *c*-type cytochrome. The formate dehydrogenase isolated from *D. desulfuricans* ATCC 27774 is homologous to *Dv*Mo-FDH and was characterized by EPR and Mössbauer spectroscopies [4]. A monoheme cytochrome, c_{553}, was identified as the physiological partner for *Dv*Mo-FDH [3, 5]. The physiological donor of *Dg*W-FDH is also a monoheme cytochrome that was recently purified (our unpublished data).

*Dg*W-FDH consists of two subunits of 977 and 214 amino acids, and it belongs to the DMSO reductase (DMSOR) family of enzymes, one of the four classes into which molybdopterin-containing enzymes have been classified [6–9]. This family is considerably broad, and, besides DMSOR [10, 11], it includes enzymes such as dissimilatory nitrate reductases (NAP) [12] and formate dehydrogenases. The members of this family have two molybdopterins (MGD cofactor) in the coordination sphere of Mo (or W), which is also bound to an amino acid side chain. This amino acid changes with the enzymatic functionality and is a serine residue in DMSOR, a cysteine in NAP, and a selenocysteine in FDHs [2, 13]. At the buried active site of *Dg*W-FDH, the tungsten atom is bound to two molybdopterin cofactors, to a selenocysteine, and to either an inorganic sulfur atom or a hydroxyl ligand. It is accessible via a positively charged tunnel, and product release may be facilitated for H^+ by buried waters and protonable amino acid side chains and for CO_2 through a hydrophobic channel conserved in other FDHs.

Results and Discussion

Primary Sequence Determination

Since no primary sequence was initially available, gene isolation, sequencing, and model building were carried out simultaneously and in an interactive manner.

For isolating the gene coding for the formate dehydrogenase large (α) subunit (*fdhA*), two degenerated oligonucleotides, CPKGASTWQ and VGDPNTIPrev, were synthesized and used to amplify, by PCR, a DNA fragment of about 2700 bp. This PCR product was cloned and sequenced by primer walking (see Experimental Procedures) and gave information about the protein sequence, 100 amino acids away from the N terminus. Furthermore, an in-frame TGA was detected in its DNA sequence, suggesting the possible presence of a selenocysteine in the *Dg*W-FDH large subunit, initially not expected [1], but revealed by crystallography [2]. Information on the flanking upstream DNA sequence was acquired by inverse PCR with primers FDH-EEKSWDWrev and FDH-NAKGQVV. The downstream DNA sequence was obtained by PCR with primers FDH-IEHPFSKT and small-CV. Assembly of the overlapping sequence fragments allowed the reconstitution of an open reading frame of 3036 bp (*fdhA*) coding for a 1012-amino acid polypeptide chain and the identification of

[3]Correspondence: mromao@dq.fct.unl.pt
[4]These authors contributed equally to this work.
[5]Present address: Crystal and Structural Chemistry, University of Utrecht, Padualaan 8, 3584 CH Utrecht, Netherlands.

Key words: tungsten; selenium; formate dehydrogenase; selenocysteine; molybdopterin; iron-sulfur cluster

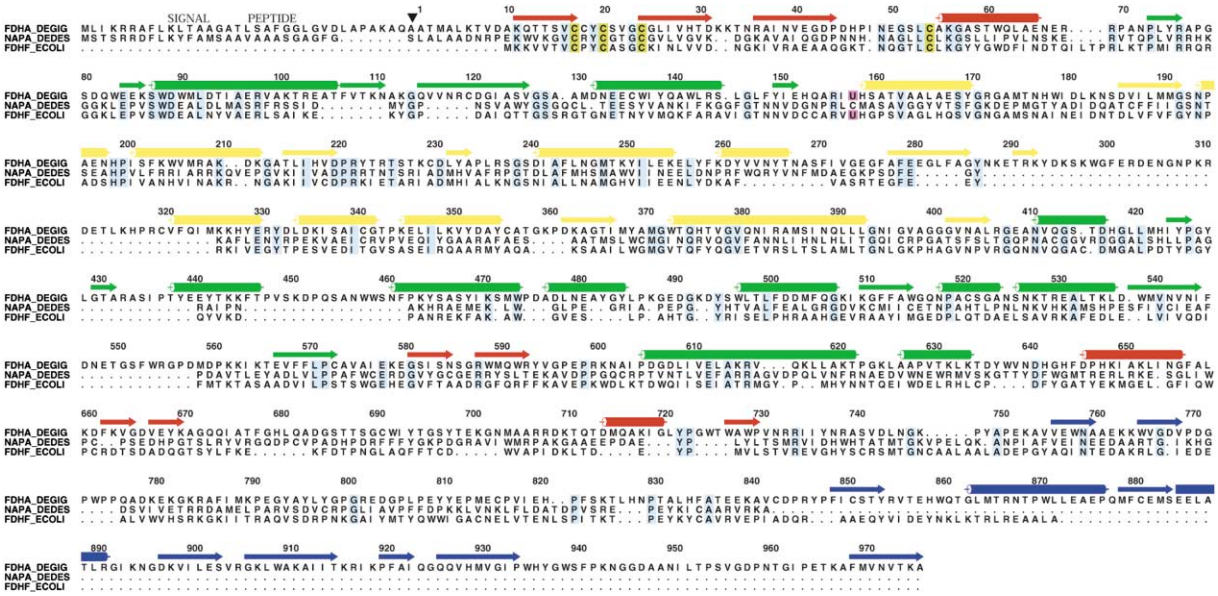

Figure 1. Amino Acid Sequence Alignment of the *Dg*W-FDH Large Subunit with Its Structural Neighbors

FDHA_DEGIG, *Dg*W-FDH α subunit, SWALL accession number Q934F5; NAPA_DEDES, NAP, SWALL accession number P88186; FDHF_ECOLI, FDH-H, SWISS-PROT accession number P07658. Conserved residues, light blue; cysteines involved in iron-sulfur cluster binding, dark yellow; selenocysteine, magenta. The secondary structural elements, β strands (→), and α helices (■) are colored according to the domains to which they belong. Domain I, red; domain II, green; domain III, yellow; domain IV, blue. ▼, signal peptide cleavage site. The residue numbering refers to the FDHA_DEGIG sequence and starts at the first residue of the mature protein. This figure was prepared with the programs PILEUP, in the Wisconsin Package Version 10.0 (Genetics Computer Group [GCG], Madison, WI), and ALSCRIPT [39].

an open reading frame coding for the formate dehydrogenase small (β) subunit (*fdhB*).

After the inclusion of the *Dg*W-FDH large subunit polypeptide sequence in the structural model available at that time, it was also possible to start tracing the polypeptide chain of the small subunit in the electron density map and to complete the sequence determined by PCR, by giving information on the C terminus.

The *fdhA* and *fdhB* sequences have been submitted to the DDBJ/EMBL/GenBank under accession numbers AJ318781 and AJ427412, respectively. The C-terminal sequence data for the formate dehydrogenase β subunit has been submitted to the SWISS-PROT Protein Data Bank under accession number P83237.

Analysis of the gene sequence revealed the features of the preprocessed *Dg*W-FDH (Figure 1). The large subunit precursor (FDHA) carries a signal peptide (the first 35 amino acid residues) with the twin-arginine motif RR-x-F-L-K [14] characteristic of Sec-independent exports to the periplasm and harbored by periplasmic molybdoproteins. The mature formate dehydrogenase large subunit is then composed of 977 residues and has a deduced molecular weight of 109,712.8 Da.

The small subunit (214 residues) has a deduced molecular weight of 23,852.0 Da and is devoid of an export signal. This strongly suggests the formation of the complex between both large and small subunits in the cytoplasm before translocation and *Dg*W-FDH export to the periplasm as an oligomeric structure, as it was demonstrated for bacterial periplasmic [Ni-Fe] hydrogenases [15].

We ran a FASTA search of our sequence data against the preliminary sequence data of the *Desulfovibrio vulgaris* Hildenborough Genome Sequencing Project, currently under processing at The Institute for Genomic Research (http://www.tigr.org), and detected two homologous FDHs in this genome. One is the already described three-subunit FDH [3], and the other is an FDH, like *Dg*W-FDH, composed only of two subunits.

Structure Solution

The initial absence of sequence information for *Dg*W-FDH was a major hurdle in solving its crystal structure. Yet a molecular replacement solution was obtained [2] with the structure from an enzyme of the same family, the periplasmic nitrate reductase (NAP) from *D. desulfuricans* [12], as a search model. This molecular replacement solution provided a model for half of the protein content, but the electron density map was of rather poor quality outside the region defined by the search model. Therefore, since the MR method did not prove to be enough to solve the structure, additional phasing information was necessary and could be obtained from a four-wavelength data set (MAD) collected at ESRF (the Fe K edge is 1.73649 Å and the inflection point is 1.74149 Å; the W L_{III} inflection point is 1.21417 Å and the remote λ is 0.992 Å). Both solutions (MR and MAD) were used to solve the structure, since the electron density maps calculated with combined MAD and model phases were of superior quality when compared to those calculated with MAD phases alone.

The model was built in several cycles of model building, phase combination with experimental phases, density modification, and tracing with ARP/wARP [16]. At first, automated tracing was unsuccessful, but it worked after strategies were used to improve both the model

Table 1. Refinement Statistics

Data resolution range (Å)	35–1.8
Number of reflections	208,782
Number of free reflections	10,979
Number of nonhydrogen protein atoms	17,783 (plus 298 double conformations) 2,382 amino acids
Number of water molecules	1,707
R factor	0.173
Free R factor	0.213
Rmsd bonds (Å)	0.019
Rmsd angles (°)	1.792
Mean B factor (Å^2) (main chain/ side chain/solvent)	(20.7/23.0/31.1)
Ramachandran plot (%)	
Favored regions	89.3
Allowed regions	10.5
Generously allowed regions	0.2
Rmsd NCS-related atoms (Å)[a]	
Cα	0.197 (without less-ordered parts)
All	0.391

[a] The rmsd values correspond to the exclusion of residues 1, 2, 837–843, and 956–966 of the large subunit; these residues are poorly defined in the electron density.

and the data. The model was significantly enhanced once the DNA corresponding to the amino acids residues 54–365 had been sequenced. Regarding the data, care was taken to include all data, not only the weak reflections (between 2.0–1.8 Å), but also those selected for the R_{free} test. Only at later stages of the refinement were these reflections omitted (R_{free}) to monitor the progress of the refinement. Additional primary sequence data were incorporated as soon as they became available. For some loops, the electron density stayed rather poor in both NCS-related molecules. Though omit maps show some density for residues 1, 2, 837–843, and 956–966 of the large subunit, these particular regions seem to be partially disordered. The two heterodimers in the asymmetric unit are essentially identical, as they can be superimposed to an RMSD of 0.39 Å for all protein atoms or 0.20 Å for all C_α atoms when the less-ordered parts are omitted (see Table 1).

Quality and Topology of the Model

Large Subunit

The *Dg*W-FDH molecule consists of two subunits. The three-dimensional structure of the large subunit (977 amino acids) harbors the W[$(MGD)_2$,-SH,-SeCys] cofactor as well as one of the [4Fe-4S] clusters and is an αβ structure, similar to the structures of FDH-H from E. *coli* [13] and to the periplasmic *D. desulfuricans* ATCC 27774 nitrate reductase (NAP) [12]. The superposition of the large subunit of *Dg*W-FDH with NAP shows an rmsd of 2.0 Å for the Cα atoms of 636 out of 723 amino acid residues. The comparison with *E. coli* FDH-H gives a corresponding rmsd of 2.1 Å for 659 out of 715 amino acids (Figure 2).

The large subunit can be divided into four domains, two of which correspond to noncontiguous stretches of the polypeptide chain, following the same classification used for FDH-H and NAP. However, *Dg*W-FDH is considerably larger than these homologous proteins (977 amino acid residues versus 723 and 715 for NAP and FDH-H, respectively), and the extra ~250 amino acids are distributed over the surface of the molecule and correspond to insertions throughout all four domains. These insertions are represented in Figure 3 as gray regions of the structure.

The N terminus (residues 1–8) of the large subunit protrudes like an arm holding the small subunit, interacting with residues Gln23, Trp24, Thr145, and Asn146 (from the small subunit) and strengthening the interaction between both subunits. Domain I (in red) is defined by residues 9–68, 575–603, and 647 –734 and, as in NAP and in FDH-H, carries the characteristic cysteine motif that binds the first [4Fe-4S] center (-$CXXCX_nCX_mC$-). When compared to the structures of NAP and FDH-H, it has a shortcut 732–733 in domain I, which replaces the hydrophilic loop 530–539 in FDH-H. Flanking this location are two inserts of domain I: residues 658–689 and 709–726 and an insert of domain IVa (740–770). These inserts, 709–726 and 740–770 on one side and insertion 658–689 on the other side, seem to define a clamp tailored to bind an α helix of the physiological partner. The proposed interface is an elongated cleft, with a diameter of 12–15 Å and a length of 30–40 Å, lined with hydrophobic and basic residues. Domain II (in green) contains 205 amino acid residues and is defined by three stretches of polypeptides, 69–157, 410–573, and 604–646. In relation to the structures of NAP and FDH-H, it contains four insertions corresponding to 71 amino acid residues (106–122, 431–466, 552–566, and 641–647). The polypeptide 431–466 defines an extended loop, which protrudes over the cleft that gives access to the buried active site. The loop 641–646 on the molecular surface makes important crystal contacts.

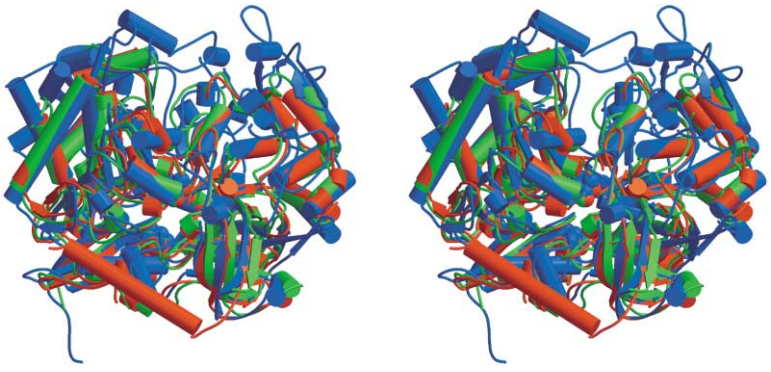

Figure 2. Superposition of the Large Subunit of *Dg*W-FDH in Blue with the Structure of the Periplasmic Nitrate Reductase from *D. desulfuricans* ATCC 27774 Represented in Green

The rmsd for the superposition of 636 amino acid residues is 2.0 Å. The structure of FDH-H from *E. coli* [13] (red) and the corresponding rmsd for 659 amino acids of *Dg*W-FDH is 2.1 Å.

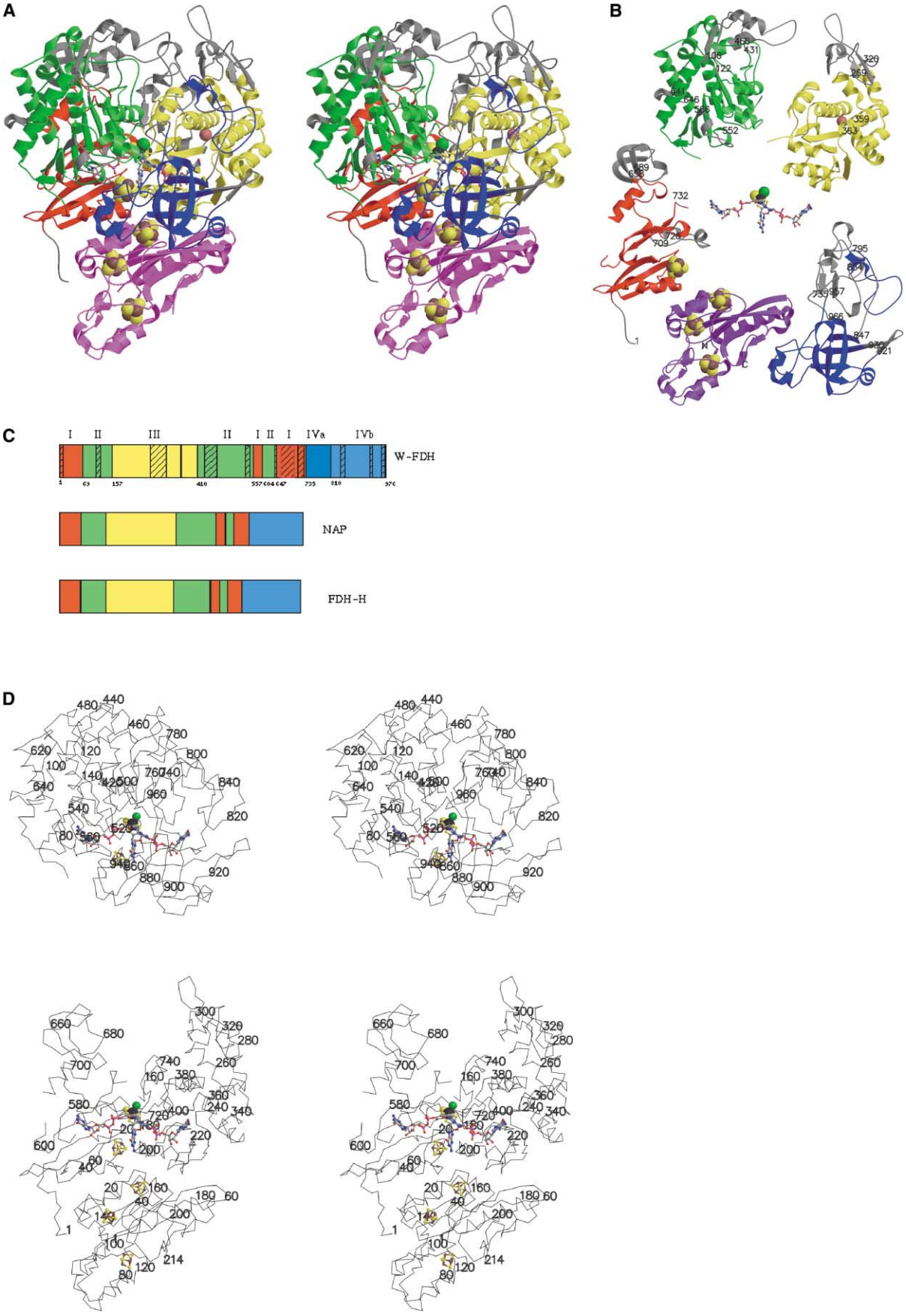
A
B
C
I
II
III
II
I II
I
IVa
IVb
W-FDH
NAP
FDH-H
D

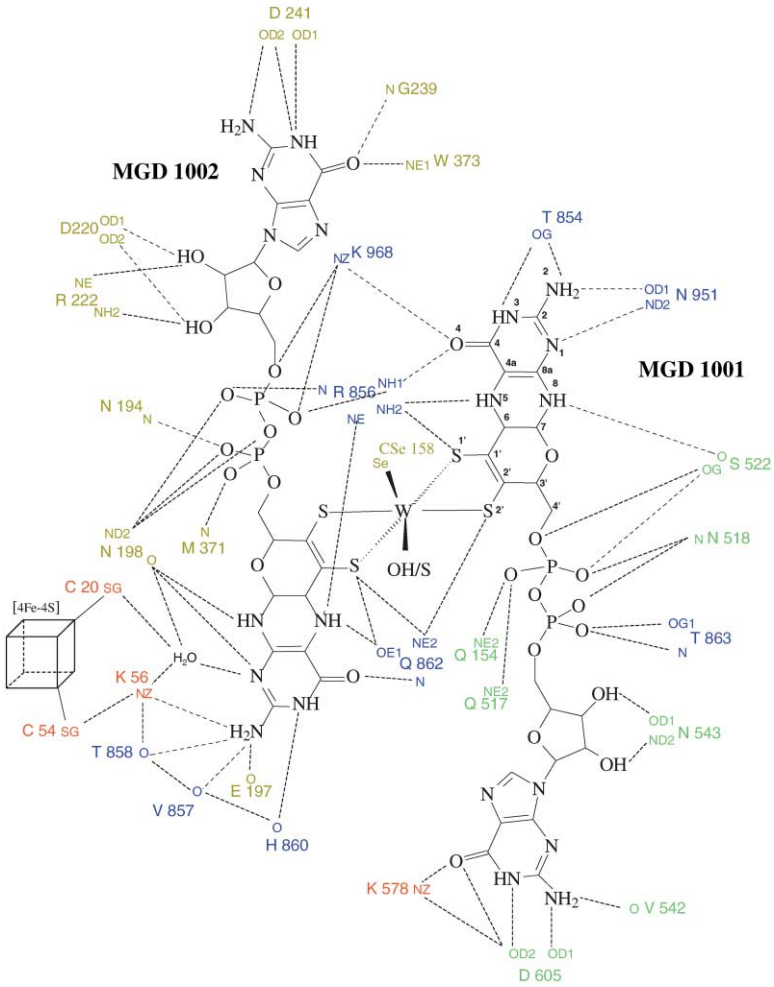

Figure 4. Schematic Representation of the Two Pyranopterin Guanosine Dinucleotide (MGD) Cofactors and the Hydrogen Bonding Interaction with Surrounding Residues and Buried Water Molecules

Hydrogen bonds were identified using CONTACT from the CCP4 package [36] and TURBO-FRODO [37].

Domain III (in yellow) is defined by a continuous polypeptide (residues 157–409) and, when compared to the structures of FDH-H and NAP, shows one long insertion of 51 amino acid residues (269–320) and a shorter one of 5 amino acids (359–363). The long insertion has an irregular secondary structure and covers the linear linker between domain IVa and IVb (795–784) with hydrophobic side chains (see below). Since it sits above the formate entrance to the active site, this tunnel is ~10 Å longer than that in FDH-H.

The insertion of residues 359–363 supplies a Ca^{2+} binding site (Figure 3A, pink sphere) that involves the backbone oxygen atoms of residues Thr358 O (2.62 Å), Lys360 O (2.92 Å), Lys363 O (2.67 Å), Leu393 O (2.68 Å), and Asp395 OD1 (2.84 Å) and a water (2.79 Å), which, in turn, is hydrogen-bonded to Pro361 O (3.12 Å) and Gly394 O (2.78 Å). The calcium ion is too far from other active parts of the protein to propose an active role for it. However, without this insertion, the interaction between Phe259 and Phe750 (absent in FDH-H and NAP) would be solvent exposed.

The C-terminal domain IV (in blue) is defined by the last 241 amino acid residues and is ca. 70 residues longer than the corresponding domain of FDH-H and NAP. Because of the large insertion 740–770, this domain can be subdivided into two subdomains connected by a linker (795–784): IVa (residues 735–795) and IVb (residues 796–977). The latter has two insertions spa-

Figure 3. Stereo Representation of the Overall Structure of *Dg*W-FDH from *D. gigas*

The small domain (214 amino acid residues) is represented in purple, and the large domain (977 amino acid residues) is colored after its domain classification. Domain I (red) corresponds to residues 9–68, 575–603, and 647–734; domain II (green) contains residues 69–157, 410–574, and 604–646; domain III (yellow) is defined by residues 157–409; domain IV (blue) is defined by residues 735–977. Domain IV can be divided into two subdomains, IVa (residues 735–795) and IVb (residues 796–977). The insertions (relative to the homologous NAP and FDH-H structures) present in several domains are shown in gray.

(B) Representation of the four "exploded" domains of the large 977 aa subunit.

(C) Comparison of the domain organization of *Dg*W-FDH, *D. desulfuricans* NAP, and *E. coli* FDH-H. The insertions in *Dg*W-FDH are depicted as dashed areas.

(D) Stereo Cα trace numbered every 20 residues for domains II and III (top).

(E) Stereo Cα trace numbered every 20 residues for domains I and IV and for the small subunit (below).

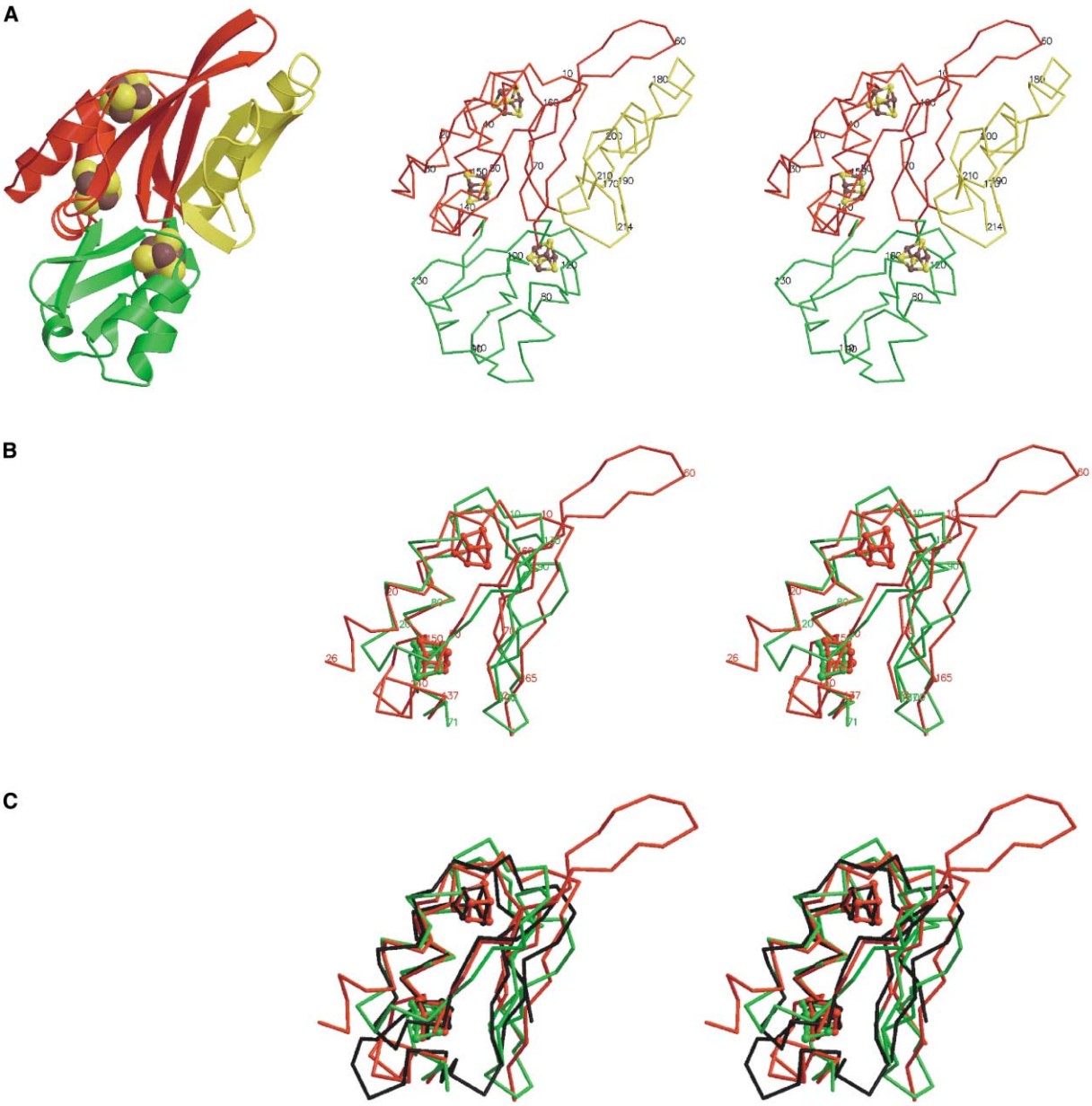

Figure 5. Small Subunit of *Dg*W-FDH

(A) Overall structure of the small subunit, as cartoon and stereo Cα trace. Domain A (red), 1–72 and 137–165; domain B (green), 73–136 (71–72 and 137 can be assigned to both domains A and B); domain C (yellow), 166–214.

(B) The ferredoxin-like domains A (red) and B (green) can be superimposed to each other with an rmsd of 1.0 Å for 31 Cα atoms plus 8 atoms from the [4Fe-4S] cluster or an rmsd of 1.1 Å for 132 main chain atoms. The domains are related by a proper rotation.

(C) Ferredoxin (Protein Data Bank entry 1blu; blue) has been superimposed on domain A (red) with an rmsd of 0.99 Å for 35 Cα atoms plus 16 [4Fe-4S] atoms. Domain B, green.

tially close together (818–843 and 921–930), while the less-ordered loop 957–966, near the active site, adopts a different orientation in FDH-H.

The only disulfide bridge, C817–C844, is located in a hydrophobic patch on the surface, close to the guanidine of MGD 1001 and is flanked by the solvent-exposed side chains of Val819, Val843, Pro846, Pro849, Phe850, and Leu891. The disulfide bridge is far away from the proposed electron transfer pathway, so it is unlikely to be actively involved in catalysis. Compared with FDH-H, residues 818–843 can be seen as an insertion, where the related chain goes through the disulfide bridge. In *Dg*W-FDH, cysteines 817 and 844 correspond topologically to FDH-H 567 and 569.

As *Dg*W-FDH needs to be activated with 2-mercaptoethanol in an anaerobic environment in order to function, it is likely that this disulphide bridge will be broken in the active form. Release of the disulfide bridge would allow wider opening and movement of the formate entry cleft and would alter the position of residues 818–848

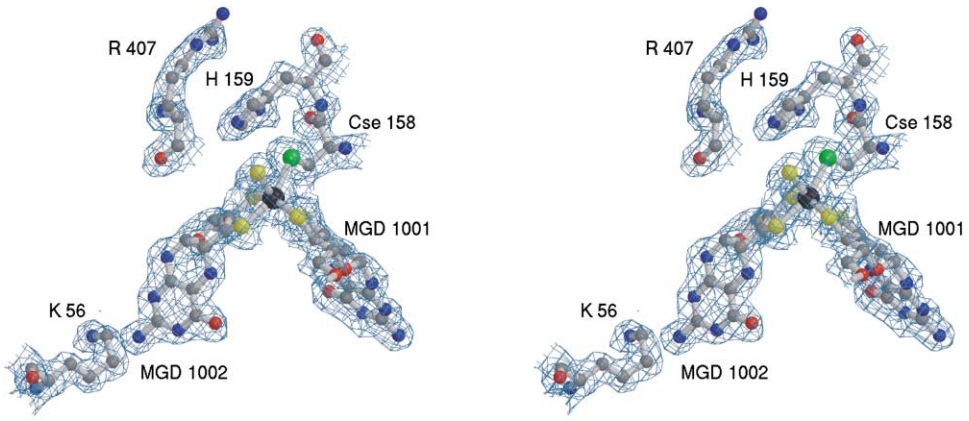

Figure 6. Representation of the Tungsten Catalytic Site of *Dg*W-FDH, Superimposed with the Final $2F_o - F_c$ Electron Density Map Contoured at 1.0 σ

Surrounding residues important for catalysis are also included: SeCys158 (bound to the W atom [black sphere]), His159, and Arg407. To the left is Lys56, which makes a hydrogen bond to the exocyclic NH_2 of MGD 1002.

(with unknown function). Maybe the disulfide bridge evolved as a protection or regulation of the enzyme to mildly oxidized (toxic) environments, contrary to FDH-H, which is permanently inactivated by oxygen [18, 19].

The C-terminal helix from FDH-H is absent, but the corresponding binding cleft in *Dg*W-FDH (ca. 40 Å long) is lined with basic and aromatic residues and might accommodate a seven-turn α helix. It might be provided by another protein to form a complex in vivo. Without such a helix, Cys156 from the small subunit, which binds [4Fe-4S] cluster 2 (the second in its relative distance to W), is solvent exposed (the most exposed from all four). This would be a suitable interaction site for the artificial electron acceptor benzylviologen, used in in vitro activity studies or for the physiological electron acceptor.

As in other enzymes from the same family, the $W(MGD)_2$ cofactor is buried at the interior of the protein and is stabilized by an extensive network of hydrogen bonding interactions to residues of mainly domains II, III, and IV (Figure 4). MGD1002 interacts with domain III and IV and with N_ξ of Lys56 of domain I. This lysine makes a bridge between the pterin and the first [4Fe-4S] cluster. The other MGD (1001) interacts with domains II and IV.

Small Subunit

The small subunit (214 amino acid residues) holds three of the iron sulfur clusters of *Dg*W-FDH (Figure 5). It is located opposite from the cleft leading to the active site and interacts with the large subunit covering a surface of ca. 2362 $Å^2$. Several hydrogen bonds, salt bridges, tightly bound waters, and hydrophobic interactions stabilize the interface between the subunits of the heterodimer. This involves over 40 residues of domains I and IV in the large subunit and 30 amino acids of the small subunit (residues 1–6, 39–41, 51–61, 229, 858, 859, 871–879, 881–883, 896, 897, and 912–918 from the large subunit and residues 11, 14, 15, 22–30, 32–38, 56, 58, 65, 141–146 and 154–157 from the small subunit). The N terminus of the large subunit wraps around the smaller subunit and contributes to the stability of the functional heterodimer. These residues may explain the increased stability of the *Dg*W-FDH complex, which allowed copurification.

The fold of the small subunit is of the $\alpha\beta$ type and contains three domains (Figure 5A): domain A (residues 1–72 and 137–165), domain B (residues 71–137), and domain C (residues 166–214). Domain A, which holds two iron-sulfur clusters, and domain B, which binds another cluster, are related by a proper 2-fold rotation. They can be superimposed to an rmsd of 0.87 Å for 26 Cα atoms and the 8 atoms of one [4Fe-4S] cluster. They are cunningly intertwined, such that some residues were assigned to both domains. The fold of domains A and B resemble 2 $\times$ [4Fe-4S] ferredoxins. With about 52 structurally conserved residues, these ferredoxins share two [4Fe-4S] clusters sandwiched between two helices on one side and a β sheet on the other side. The 2 $\times$ [4Fe-4S] ferredoxin from *Chromatium vinosum* (Protein Data Bank entry 1blu; [20]), for example, can be superimposed to an rmsd of 0.99 Å for 35 Cα atoms (out of 82) and 16 atoms of the metal clusters (2 $\times$ [4Fe-4S]) (Figure 5C). The two helices and the [4Fe-4S] clusters fit particularly well. Similar results are obtained with other ferredoxins. Even the Fe-only hydrogenase from *Desulfovibrio desulfuricans* (Protein Data Bank entry 1hfe [21]) can be superimposed to 0.68 Å for 29 Cα atoms (the region of Hase around Fe-S clusters 422 and 423) and atoms from these 2 $\times$ [4Fe-4S] clusters.

During the latest stages in the preparation of this manuscript, the *E. coli* FDH-N structure was published [22]. In this structure the β subunit harbors four [4Fe-4S] clusters. Interestingly, as already advanced by us (our unpublished data), there is space and the correct fold for an additional [4Fe-4S] cluster in the *Dg*W-FDH small subunit, which would be present if the residues Ala84-xn-Leu110-xx-Tyr113-xx-Val116 were mutated to Cys. The FeS-3 cluster present in FDH-N [22] is the experimental evidence that corroborates our former prediction. Furthermore, the same motif found in the *E. coli* FDH-N is conserved in all sequences of FDHs currently available in the database.

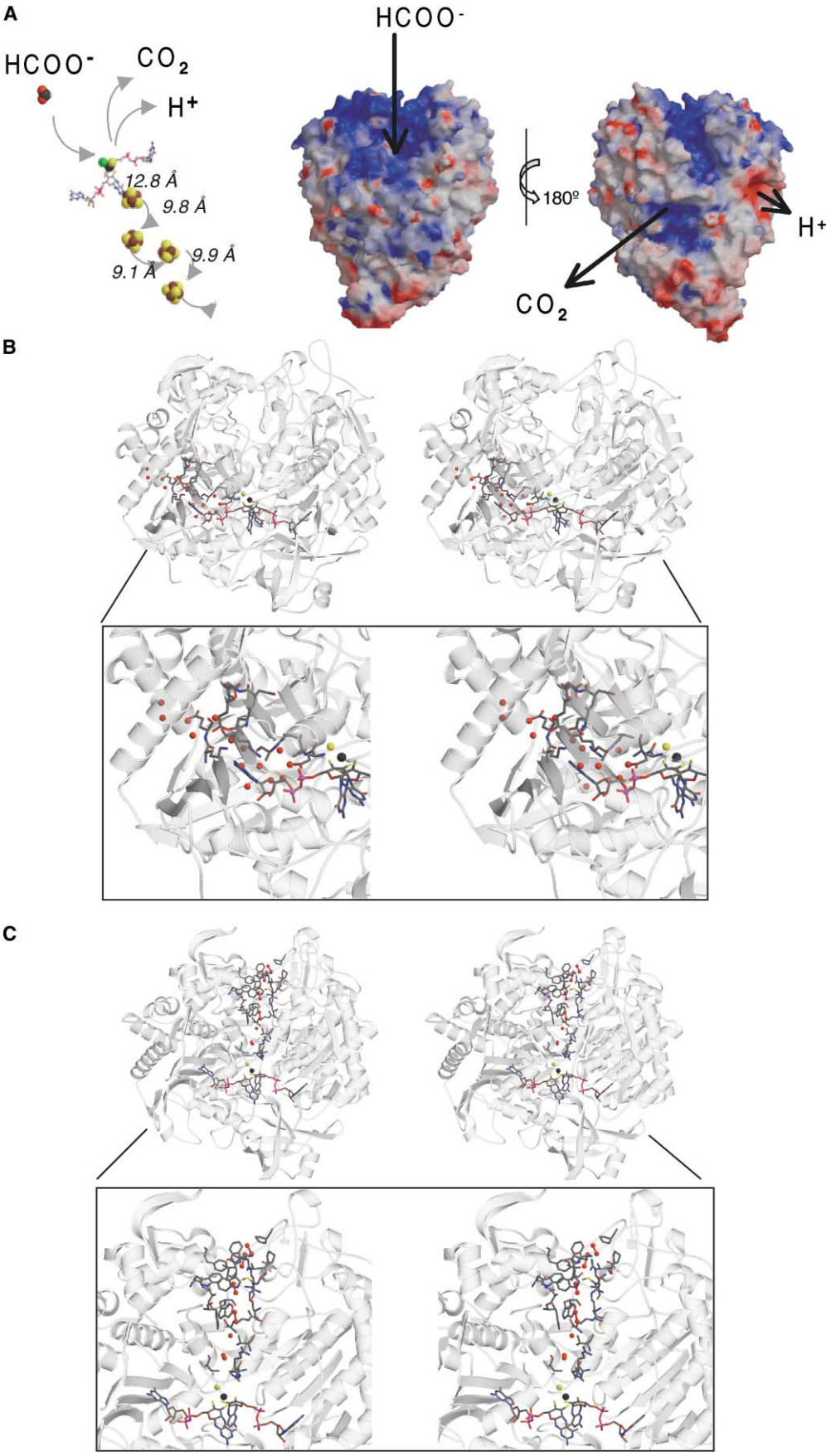
A
HCOO-
CO2
H+
12.8 Å
9.8 Å
9.9 Å
9.1 Å
HCOO-
180º
H+
CO2
B
C

Tungsten Site and Coordinating Ligands

In the crystallized form of the enzyme, the W atom is coordinated to the four dithiolate sulfur atoms from the two MGDs, by the selenium atom of SeCys158 and by one hydroxyl or sulfide ligand (Figure 6). In the vicinity of the buried W site, similarly to *E. coli* FDH-H, are His159, probably directly involved in the enzymatic mechanism (as proposed by EPR for FDH-H [18]), and Arg 407, which points toward the entry of the tunnel and may be responsible for orienting the substrate molecule.

The dithiolene function of both MGD cofactors is expected to be flat (double bonded), as found in other molybdopterin-containing enzymes [10–13, 17]. This seems to be true for MGD1002, but, in MGD1001, it refines better when restraints for the reduced form [C12′(R)-C13′(R)] are applied.

The sixth tungsten ligand, supposedly an oxygen ligand, as proposed also for FDH-H [10, 14], behaved poorly in refinement, giving rise to a peak (>5 σ) in an $mF_o - DF_c$ difference electron density map. Besides, the B factor for an OH ligand was only half that from the tungsten atom: 11.6/20.6 Å^2 and 10.8/20.6 Å^2 for both NCS monomers. If refined as a sulfur atom, the corresponding temperature factors were of the same magnitude as those from surrounding atoms, with B factors for S/W of 25.1/20.8 Å^2 and 24.7/20.6 Å^2 for both independent molecules. In this case, the bond distance W-SH (unrestrained) refined to 2.41 Å, a typical value for this type of bond and too long for a W-OH bond distance, and the spurious difference electron density peak disappeared. Further anisotropic refinement of the sixth tungsten ligand showed that it possesses a large anisotropy, i.e., more angular freedom than bond length variations. Taking this anisotropy (assuming an OH ligand) into account lead to B factors of 14.0 Å^2, instead of 11 Å^2, compared to 15.6–19.0 Å^2 for the MGD-sulfur atoms and 20.7 Å^2 for the W atom. This seems suggestively low, though it might be attributed to experimental error. Such anisotropic refinement of the O ligand has not been carried out for related structures with low B factors for their OH ligands (e.g., FDH-H [13]). Also suggestive are the bond distance W-OH, which stays at 2.41 Å, and the distance from the hydrogen bond to the backbone N of Glu409 at 3.6 Å, which is too long for a hydroxide, but would be acceptable for a sulfur ligand. In the case of the NAP structure [12], although the difference in the relative B factors between Mo and the OH ligand was not significant (27 Å^2/31 Å^2 for OH/Mo), there was always a residual electron density of ~6 σ, close to the OH ligand. When the latter was refined as a sulfur atom, the Mo-S distance refined to 2.39 Å, and the positive residual density vanished. In this case the B factors were 37 Å^2/30 Å^2 for S/Mo (our unpublished data).

As has been demonstrated by activity experiments of *E. coli* FDH-H using ^{13}C-labeled formate in ^{18}O-enriched water [18], the reaction catalyzed does not involve an oxygen transfer. Therefore, a putative reaction mechanism could make more sense with a sulfur ligand to W. Although EXAFS data seem to favor the OH ligand for FDH-H [19], these data are not conclusive, probably because it is difficult to distinguish similar ligands with different distances in EXAFS [G. George, personal communication]. Our crystallographic data favor a sulfur atom for the sixth ligand, although the resolution of the data does not permit us to discriminate unambiguously between O and S until higher resolution data are available or until decisive biochemical assays settle the argument.

How *Dg*W-FDH Works

The Active Site and Substrate Access

The active site of *Dg*W-FDH is buried and ca. 25 Å away from the molecular surface. However, as in other molybdopterin-containing enzymes, there is a clear funnel-shaped entrance that leads access to the internal active site. From a careful analysis of the *Dg*W-FDH structure, one is tempted to assign functions to structural peculiarities. The formate molecule could easily reach the buried active site through the tunnel (Figure 7A), which is positively lined with His159, Arg156, His423 His963, His376, Lys791, Lys444, Lys445, Arg587, and Arg407. At the bottom of this channel is the W active site (Figure 6), which resembles the Mo site of the homologous FDH-H from *E. coli* [13]. His159 (His141 in FDH-H) is an important active site residue and establishes a π interaction with the Se atom of the metal ligand Se-Cys158. Besides, there is a clear pH dependency in the catalytic activity, for FDH-H [13,18] as well as for *Dg*W-FDH (our unpublished data), and protonation of this histidine residue by the α proton of formate has been proposed for FDH-H, supported by EPR studies [18, 19]. Arg407 (Arg333 in FDH-H) provides a positive charge and a hydrogen bond to orient the substrate molecule for catalysis.

Putative Proton Channel

The enzymatic reaction involves the release of H^+, and there is a putative proton channel, which connects the active site to the exterior of the FDH molecule. It is located almost perpendicular to the "formate cleft", as depicted on the surface electrostatic potential represen-

Figure 7. How *Dg*W-FDH Works

(A) Diagram of *Dg*W-FDH cofactors and GRASP [38] electrostatic-potential surface plot contoured for positive charges (blue) and negative charges (red). The top cleft is lined with basic amino acids and provides an excellent entry point for the formate. At the W/Se center, the formate is split into CO_2, H^+, and two electrons. To the left are the four [4Fe-4S] clusters. Counting at increasing distance from W: [4Fe-4S] 1 (large subunit) Cys17-xx-20-xxx-24-x_n-54; [4Fe-4S] 2 (small subunit) Cys11-xx-Cys14-xx-Cys17-x_n-156; [4Fe-4S] 3 Cys21-x_n-Cys137-xx-Cys140-x_n-152; [4Fe-4S] 4 Cys72-xx-Cys75-xxxx-Cys80-x_n-Cys120. There would be space and the correct fold for a fifth [4Fe-4S] if the residues Ala84-xn-Leu110-xx-Tyr113-xx-Val116 were mutated to Cys.

(B) A chain of water and protonable residues provides a channel from the reaction center to the surface of the FDH. The orientation of the picture is similar to that of Figure 7A, middle and left.

(C) More or less perpendicular to the formate entry and the proton channel is channel lined with aromatic and hydrogen bond-donating residues. Putative CO_2 binding sites are indicated with sticks between observed water molecules (red). The picture has been rotated ~20° around the horizontal axis and ~35° around the vertical axis relative to Figure 7B.

tations (Figure 7B), and is coated with protonable amino acid side chains (Glu409, Asp132, Glu134, and Glu579) and a chain of water molecules.

Not all of these residues are conserved in FDH-H. An alternative pathway in FDH-H may involve phosphates and the guanine of MGD-801. These differences may be due to the different cell location of both enzymes (different pH environment), since, while *Dg*W-FDH is present in the periplasmic space, the *E. coli* FDH-H is located in the cytoplasm.

Putative CO_2 Channel

The release of the product molecule CO_2 from the buried active site may be facilitated by a hydrophobic channel, which is coated by several H bond-donating amino acid residues (Figure 7C). The residues Val412, His159, Trp730, and Tyr428 are conserved in FDH-H (Val338, His141, Trp528, and Tyr354). Other amino acids from this channel (Arg172, Arg734, Trp458, Trp693, Trp730, and Trp459), which are closer to the molecular surface, correspond to one of the insertions in *Dg*W-FDH, being absent in the smaller FDH-H, and, consequently, the equivalent channel is much shorter. Both Arg172 and Arg734 donate bidentate hydrogen bonds to what could be a CO_2 binding site, perpendicular to the plane of the tryptophan side chain, clamping the CO_2 between them. (Figure 7C).

In respect to the differences between FDH-H and *Dg*W-FDH, the CO_2 channel is longer and more selective in *Dg*W-FDH as well as in the formate entry, which is ~10 Å deeper. One possible explanation may be that more specific and longer channels are needed to protect the active site of *Dg*W-FDH because of its location in the periplasmic space, where more undefined molecules may interact with (and eventually block) the enzyme.

Electron Transfer Pathway

As found in other enzymes from the same family, the electron transfer involves just one of the pterins (MGD 1002). The closest pathway between the pteridine moiety and the nearest [4Fe-4S] center is mediated by the Nζ of Lys56 (Lys44 in FDH-H and Lys49 in NAP), which makes a favorable hydrogen bond with the exocyclic NH_2 of the pyranopterin (Figures 4 and 6). This electron transfer pathway via the exocyclic NH_2 is found not only in the enzymes from the DMSOR family (NAP and FDH-H), but also in the enzymes from the xanthine oxidase family (MOP [17] and xanthine oxidase [23]), although, in the latter case, the closest contact is to the Sγ of one cysteine residue from the nearest [2Fe-2S] center. All four [4Fe-4S] clusters are 9 to 10 Å apart [2] (Figure 7A), providing an easy electron pathway to the physiological electron donor (monoheme cytochrome) of *Dg*W-FDH.

Biological Implications

In contrast to the related molybdoenzyme FDH-H [13], which is composed of a single polypeptide chain, and to molybdenum-containing formate dehydrogenases of the *Desulfovibrio* species [3, 4], which are complexes of three different subunits, the tungsten enzyme from *D. gigas*, *Dg*W-FDH, is a heterodimer. The complex is composed of a large subunit carrying the W active site, one [4Fe-4S] center (in an arrangement resembling the related monomeric enzymes FDH-H [13] and NAP [12]), and a small subunit that harbors a series of three [4Fe-4S] clusters as well as a putative vacant binding site for a fourth cluster.

Recently, the sequences of two other tungsten formate dehydrogenases became available in the databases. FDH-I and FDH-II from *Eubacterium acidaminophilum* are also heterodimers (SWALL accession numbers for the respective subunits are Q93V06 and Q93SF5 and Q93V05 and Q93SF1), but no significant sequence similarity with *Dg*W-FDH was found. A specific tungsten ABC transporter, discriminating molybdenum, was reported for this mesophile last year [24], and, so far, no molybdenum-dependent enzymes have been detected. On the contrary, molybdenum enzymes, such as the aldehyde oxidoreductase (MOP) [17], and tungsten enzymes, such as the *Dg*W-FDH [1], have been isolated from cultures of *D. gigas* grown under identical conditions. Since Mo is a more versatile element than W and Mo-containing centers have higher redox potentials [25], the sulfate reducer *D. gigas* can be regarded as a mesophilic organism representative of a transition from a "W world" to a "Mo world", which would correspond to the adaptation to more oxidized environments.

Experimental Procedures

Gene Sequence Determination

Unless otherwise mentioned, standard molecular biology protocols were used [27]. Oligonucleotides CPKGASTWQ, 5′-TGYCCIAARG GIGCIWSIACITGGCA-3′, and VGDPNTGIrev, 5′-GGIATIGTRTTIG GRTCICCIAC-3′, were synthesized on the basis of on the formate dehydrogenase large (α) subunit internal peptides CPKGASTWQLAENERRPANPLYRAPGSDQ and TPSVGDPNTGIPETK and used to amplify, by PCR, a 2700 bp DNA fragment of the corresponding gene (*fdhA*). The resulting product was cloned in pPCR-Script Amp SK (+) (Stratagene) and sequenced with primers T3 and T7 (New England Biolabs) and by primer walking, with an automated DNA sequencer (Model 373; Applied Biosystems, Forster City, CA) and the PRISM ready reaction dye deoxy terminator cycle sequencing kit (Applied Biosystems). From the obtained DNA sequence, we designed the "inside-out" primers FDH-EEKSWDWrev, 5′-AGTCC CAGCTTTTTTCTTCCC-3′, and FDH-NAKGQVV, 5′-ATGGACAAC GAAGAGTGCTG-3′, for inverse PCR DNA amplification of the missing flanking regions [26–29]. Attempts to amplify the downstream region with this technique were not successful, so it was just used to acquire information on the upstream region. On the basis of a restriction enzyme map of the known *fdhA* sequence, the restriction enzyme AvaI (New England Biolabs) was chosen for hydrolysis of 1 μg genomic DNA in a volume of 200 μl. After incubation for 1 hr 30 min, the enzyme was heat inactivated for 20 min at 70°C. The restriction fragments were then diluted 100-fold, and 530 μl were ligated with 28 U of T4 DNA ligase (New England Biolabs) for 16 hr at 4°C in a total volume of 600 μl. Using 14.5 μl of these DNA circles as templates, 50 pmol of each primer, and 2.5 U Herculase (Stratagene) in 25 μl reaction mixture, we obtained a PCR product of about 1500 bp. The PCR product was directly sequenced.

The downstream sequence was obtained by PCR with primers FDH-IEHPFSKT, 5′-CATCGAGCATCCCTTCTCCAAG-3′ (internal to *fdhA*), and small CV, 5′-ACCGGTGGGGCAGGTCTTCACGCA-3′, on the basis of the amino acid sequence CVKTCPTG, conserved in the formate dehydrogenases iron-sulfur (β) subunits currently available in the databases and predicted by us from the preliminary sequence data of the *Desulfovibrio vulgaris* Hildenborough Genome Sequencing Project, accessible at The Institute for Genomic Research Website (http://www.tigr.org). *D. gigas* codon usage was taken into account when we used this approach. A 1000 bp product was obtained and directly sequenced.

Assembly of the overlapping sequence fragments allowed the reconstitution of an open reading frame of 3036 bp (*fdhA*), coding for a 1012-amino acid polypeptide chain and the identification of an open reading frame coding for the formate dehydrogenase small (β) subunit (*fdhB*). A signal peptide harboring the twin-arginine motif was detected in the large subunit, and its cleavage site was predicted with Signal P (http://www.cbs.dtu.dk) [30]. The molecular weights of the mature polypeptide chains were calculated with the ProtParam tool (http://www.expasy.org/tools/protparam.html).

Protein Purification

Purification of *D. gigas* formate dehydrogenase was performed according to the procedure described in previous publications [1, 2]. The purification scheme included two steps of ion exchange chromatography (DEAE-52 and Source 15), a gel filtration step (Superdex 200), and another step on an ion exchange column (Source 15). The remaining impurities precipitated with the addition of isopropanol to a final concentration of 30%.

Crystallization, Data Collection, and Reprocessing

The crystallization conditions and data collection of *Dg*W-FDH are described in reference [2]. *Dg*W-FDH ($\sim$10 g/l) was crystallized in sitting drops. Red-brown needle-shaped crystals grew in 2–7 days at 4°C in drops containing 0.1 M HEPES (pH 7.5), 20% (w/v) PEG 3350, 10% (v/v) isopropanol, and 1% β-octylglucoside. Only very pure protein batches crystallized, and they were further improved through macroseeding techniques. All data were collected at 100 K using 10% PEG 400 as a cryoprotectant.

A four-wavelength MAD data set, collected at the BM-14 beam line at ESRF, was used to obtain phases: the Fe K edge, 1.73649 Å, and inflection point, 1.74149 Å, and the W L_{III} inflection point, 1.21417 Å, and remote wavelength, 0.992 Å, which were used for refinement. The data were processed with Denzo and Scalepack [31] in space group $P2_1$, with cell dimensions a = 73.4 Å, b = 110.4 Å, c = 156.2 Å, and β = 93.5°, which allows for two molecules in the asymmetric unit (V_M = 2.65 Å^3/Da). The crystals diffracted up to 2.7 Å at the iron K edge, to 2.15 Å at the tungsten L_{III} edge, and to 2.0 Å near the tungsten L_I edge (λ = 0.992 Å), defined by a 2 I/σ cutoff. Data collected at the latter wavelength were used for refinement but were reprocessed to include all reflections between 2.0 and 1.8 Å. Even though the statistics of the extra data were rather poor, they were essential for ARP/wARP [16], in order to build parts of the model automatically.

Phasing and Model Building

Both tungsten atom positions were located with Patterson methods, while iron and selenium positions were identified in phased dispersive difference maps. Multiple-wavelength (MAD) phases (SHARP [32]) were combined with the molecular replacement (MR) solution that was obtained with the nitrate reductase from *D. desulfuricans* [12] as a search model. The resulting phases were further improved, as described elsewhere in detail [2]. After manual rebuilding, ARP/wARP was able to build parts of the structure automatically when all data up to 1.8 Å were used, i.e., it was essential not to exclude reflections for R_{free}. About 700 out of 2 $\times$ (977 + 214) amino acids were found initially and used to rebuild the model with the program O [33, 34]. Amino acid side chains were first built in as alanine, glycine, or serine residues, except in those regions where the electron density was beyond any doubt or for which the DNA sequence had already been determined. The two NCS monomers were assumed to be identical, and parts that were clear in one molecule were also used in the other. The resulting model was used for phase combination with the experimental MAD phases, and it was used as an improved input for ARP/wARP. After several rounds of such cycles, the model was completed manually. Further refinement was carried out with Refmac5 [35], while ARP was employed for updating the water molecules. NCS restraints were maintained throughout refinement, except for 47 amino acids that differed clearly.

Initially, the $mF_o - DF_c$ maps showed large difference peaks at the W-Se site. This was alleviated at the later stages of the refinement when all distance restraints to the W were released, and W, Se, and MGD-sulfur atoms were refined anisotropically. The W-Se distance was refined without restraints, and the final bond distances were 2.54 Å and 2.55 Å for the two *Dg*W-FDH molecules.

Initial restraints on the [4Fe-4S] clusters proved to be too tight and were loosened considerably. In the final refinement, only loose restraints on the Fe-S distances and Fe-S-Fe and S-Fe-S angles were applied (d = 2.4 Å, σ = 0.08 Å, Fe-S-Fe = 72.5°, σ = 5°, S-Fe-S = 106°, and σ = 5°). Anisotropic refinement did not improve the quality of the corresponding electron density maps or the R_{free} and was not applied in the final refinement.

The dithiolene function of the MGD cofactor was restrained to be flat in MGD 1002, but, in MGD 1001, restraints for the corresponding reduced form (dithiolate in alternate conformation) described the electron density better. The difference can be attributed to the propagation of angle and bond length restraints, since the differences in the MGD C12 and C13 positions are relatively small (0.35 Å) when compared to the resolution of the data. The fact that $2mF_o - DF_c$ and $mF_o - F_c$ maps improved locally was decisive.

Acknowledgments

This work was supported by EC-TMR/FMRX-CT980204, PhD grant PRAXISXXI/BD/16009/98 (S.M.), and PhD grant PRAXISXXI/BD/13530/97 (J.M.D.). We thank the EMBL Grenoble Outstation, beamline BM-14, for MAD measurements at the ESRF under the European Union TMR/LSF Program. Hans Bartunik and Gleb Bourenkov are acknowledged for help at the BW6 beamline of the MPG-ASMB in DESY, Hamburg, for collecting the first FDH native data set. The Institute for Genomic Research (TIGR) is kindly acknowledged for making the preliminary sequence data on the *Desulfovibrio vulgaris* Hildenborough genome available to the public at their Website (http://www.tigr.org).

Received: March 28, 2002
Revised: May 2, 2002
Accepted: July 1, 2002

References

1. Almendra, M.J., Brondino, C.D., Gavel, O., Pereira, A.S., Tavares, P., Bursakov, S., Duarte, R., Caldeira, J., Moura, J.J.G., and Moura, I. (1999). Purification and characterization of a tungsten-containing formate dehydrogenase from *Desulfovibrio gigas*. Biochemistry *38*, 16366–16372.
2. Raaijmakers, H., Teixeira, S., Dias, J.M., Almendra, M.J., Brondino, C.D., Moura, I., Moura, J.J.G., and Romão, M.J. (2001). Tungsten-containing formate dehydrogenase from *Desulfovibrio gigas*: metal identification and preliminary structural data by multi-wavelength crystallography. J. Biol. Inorg. Chem. *6*, 398–404.
3. Sebban, C., Blanchard, L., Bruschi, M., and Guerslequin, F. (1995). Purification and characterization of the formate dehydrogenase from *Desulfovibrio vulgaris* Hildenborough. FEMS Microbiol. Lett. *133*, 143–149.
4. Costa, C., Teixeira, M., LeGall, J., Moura, J.J.G., and Moura, I. (1997). Formate dehydrogenase from *Desulfovibrio desulfuricans* ATCC 27774: isolation and spectroscopic characterization of the active sites (heme, iron-sulfur centres and molybdenum). J. Biol. Inorg. Chem. *2*, 198–208.
5. Sebban-Kreuzer, C., Dola, A., and Guerlesquin, F. (1998). The formate dehydrogenase-cytochrome c_{553} complex from *Desulfovibrio vulgaris* Hildenborough. Eur. J. Biochem. *253*, 645–652.
6. Romão, M.J., Moura, J.J.G., Knäblein, J., and Huber, R. (1997). Structure and function of molybdopterin containing enzymes. Prog. Biophys. Mol. Biol. *68*, 121–144.
7. Romão, M.J., and Huber, R. (1998). Structure and function of the xanthine-oxidase family of molybdenum enzymes. In Metal Sites in Proteins and Models—Redox Centers, Structure and Bonding, H.A.O. Hill, A.J. Sadler, and A.J. Thomson, eds. (Berlin: Springer-Verlag), pp. 69–96
8. Hille, R. (1996). The mononuclear molybdenum enzymes. Chem. Rev. *96*, 2757–2816.
9. Kisker, C., Schindelin, H., and Rees, D.C. (1997). Molybdenum-

cofactor containing enzymes: structure and mechanism. Annu. Rev. Biochem. *66*, 233–267.
10. Schneider, F., Löwe, J., Huber, R., Schindelin, H., Kisker, C., and Knäblein, J. (1996). Crystal structure of dimethyl sulfoxide reductase from *Rhodobacter capsulatus* at 1.88 Å resolution. J. Mol. Biol. *263*, 53–69.
11. Schindelin, H., Kisker, C., Hilton, J., Rajagopalan, K.V., and Rees, D.C. (1996). Crystal structure of DMSO reductase: redox-linked changes in molybdopterin coordination. Science *272*, 1615–1621.
12. Dias, J.M., Than, M.E., Humm, A., Huber, R., Bourenkov, G.P., Bartunik, H.D., Bursakov, S., Calvete, J., Caldeira, J., Carneiro, C., et al. (1999). Crystal structure of the first dissimilatory nitrate reductase at 1.9 Å solved by MAD methods. Structure *7*, 65–79.
13. Boyington, J.C., Gladyshev, V.N., Khangulov, S.V., Stadtman, T.C., and Sun, P.D. (1997). Crystal structure of formate dehydrogenase H: catalysis involving Mo, molybdopterin, selenocysteine, and a [4Fe-4S] cluster. Science *275*, 1305–1308.
14. Berks, B. (1996). A common export pathway for proteins binding complex redox cofactors? Mol. Microbiol. *22*, 393–404.
15. Rodrigue, A., Chanal, A., Beck, K., Müller, M., and Wu, L.-F. (1999). Co-translocation of a periplasmic enzyme complex by a hitchhiker mechanism through the bacterial Tat Pathway. J. Biol. Chem. *274*, 13223–13228.
16. Perrakis, A., Morris, R.J., and Lamzin, V.S. (1999). Automated protein model building combined with iterative structure refinement. Nat. Struct. Biol. *6*, 458–463.
17. Romão, M.J., Archer, M., Moura, I., Moura, J.J.G., LeGall, J., Engh, R., Schneider, M., Hof, P., and Huber, R. (1995). Crystal Structure of the xanthine oxidase-related aldehyde oxido-reductase from *D. gigas*. Science *167*, 1170–1176.
18. Khangulov, S.V., Gladyshev, V.N., Dismukes, G.C., and Stadtman, T.C. (1998). Selenium-containing formate dehydrogenase H from *Escherichia coli*: a molybdopterin enzyme that catalyses formate oxidation without oxygen transfer. Biochemistry *37*, 3518–3528.
19. George, G.N., Colangelo, C.M., Dong, J., Scott, R.A., Khangulov, S.V., Gladyshev, V.N., and Stadtman, T.C. (1998). X-ray absorption spectroscopy of the molybdenum site of *Escherichia coli* formate dehydrogenase. J. Am. Chem. Soc. *120*, 1267–1273.
20. Moulis, J.M., Sieker, L.C., Wilson, K.S., and Dauter, Z. (1996). Crystal structure of the 2[4Fe-4S] ferredoxin from *Chromatium vinosum*: evolutionary and mechanistic inferences for [3/4Fe-4S] ferredoxins. Protein Sci. *5*, 1765–1775.
21. Nicolet, Y., Piras, C., Legrand, P., Hatchikian, E.C., and Fontecilla-Camps, J.C. (1999). *Desulfovibrio desulfuricans* iron hydrogenase: the structure shows unusual coordination to an active site Fe binuclear center. Structure *7*, 13–23.
22. Jormakka, M., Törnroth, S., Byrne, B., and Iwata, S. (2002). Molecular basis of proton motive force generation: structure of formate dehydrogenase-N. Science *295*, 1863–1868.
23. Enroth, C., Eger, B.T., Okamoto, K., Nishino, T., Nishino, T., and Pai, E.F. (2000). Crystal structures of bovine milk xanthine dehydrogenase and xanthine oxidase: structure-based mechanism of conversion. Proc. Natl. Acad. Sci. USA *97*, 10723–10728.
24. Makdessi, K., Andreesen, J.R., and Pich, A. (2001). Tungstate uptake by a highly specific ABC transporter in *Eubacterium acidaminophilum*. J. Biol. Chem. *276*, 24557–24564.
25. Kletzin, A., and Adams, M.W. (1996). Tungsten in biological systems. FEMS Microbiol. Rev. *18*, 5–63.
26. Sambrook, J., Fritsch, E.F., and Maniatis, T. (1989). Molecular Cloning—A Laboratory Manual, Second Edition (Cold Spring Harbor, New York: Cold Spring Harbor Laboratory Press).
27. Ochman, H., Gerber, A.S., and Hartl, D.L. (1988). Genetic applications of an inverse polymerase chain reaction. Genetics *120*, 621–623.
28. Triglia, T., Peterson, M.G., and Kemp, D.J. (1988). A procedure for in vitro amplification of DNA segments that lie outside the boundaries of known sequences. Nucleic Acids Res. *16*, 8186.
29. Silver, J., and Keerikatte, V. (1989). Novel use of the polymerase chain reaction to amplify cellular DNA adjacent to an integrated provirus. J. Virol. *63*, 1924–1928.
30. Nielsen, H., Engelbrecht, J., Brunak, S., and von Heijne, G. (1997). Identification of prokaryotic and eukaryotic signal peptides and prediction of their cleavage sites. Protein Eng. *10*, 1–6.
31. Otwinowski, Z., and Minor, W. (1997). Processing of X-ray diffraction data collected in oscillation mode. In Methods in Enzymology, Volume 276: Macromolecular Crystallography, Part A, C.W. Carter, Jr., and R.M. Sweet, eds. (New York: Academic Press), pp. 307–326.
32. de La Fortelle, E., and Bricogne, G. (1997). Maximum-likelihood heavy-atom parameter refinement for multiple isomorphous replacement and multiwavelength anomalous diffraction methods. Methods Enzymol. *276*, 472–494.
33. Jones, T.A., Zou, J.-Y., Cowan, S.W., and Kjeldgaard, M. (1991). Improved methods for building protein models in electron density maps and the location of errors in these models. Acta Crystallogr. A *47*, 110–119.
34. Kleywegt, G.J., and Jones, T.A. (1996). OOPS—efficient rebuilding of protein structures. Acta Crystallogr. D Biol. Crystallogr. *52*, 829–832.
35. Murshudov, G.N., Vagin, A.A., and Dodson, E.J. (1997). Refinement of macromolecular structures by the maximum-likelihood method. Acta Crystallogr. D Biol. Crystallogr. *53*, 240–255.
36. Collaborative Computational Project, Number 4. (1994). The CCP4 suite: programs for protein crystallography. Acta Crystallogr. D Biol. Crystallogr. *50*, 760–763.
37. Roussel, A., and Cambilau, C. (1989). TURBO-FRODO, molecular modeling package. In Silicon Graphics Geometry Partner Directory (Mountain View, CA: Silicon Graphics), pp. 77–78.
38. Nicholls, A., Sharp, K., and Honig, B. (1991). Protein folding and association: insights from the interfacial and thermodynamic properties of hydrocarbons. Proteins *11*, 134–138.
39. Barton, G.J. (1993). ALSCRIPT—a tool to format multiple sequence alignments. Protein Eng. *6*, 37–40.

Accession Numbers

The atomic coordinates and structure factors have been deposited in the Protein Data Bank with the entry codes 1h0h and r1h0hsf, respectively.